IMPACT OF LOADING DISTRIBUTION OF ABRAMS SUSPENSION ON TRACK PERFORMANCE AND DURABILITY

David Ostberg
Bill Bradford
US Army Tank-Automotive Research Development and Engineering Center (TARDEC)
Ground Vehicle Power and Mobility (GVP&M)
Warren, MI

ABSTRACT

High life cycle costs coupled with durability and environmental challenges of tracked vehicles in South West Asia (SWA) have focused R&D activities on understanding failure modes of track components as well as understanding the system impacts on track durability.

The durability limiters for M1 Abrams (M1, M1A1, and M1A2) T-158LL track systems are the elastomeric components.

The focus of this study is to review test methodology utilized to collect preliminary data on the loading distribution of a static vehicle. Proposed design changes and path forward for prediction of durability of elastomers at the systems level from component testing will be presented.

INTRODUCTION

Programmatic Background

TARDEC GVP&M Track & Suspension (T&S) team was tasked by Program Manager (PM) Heavy Brigade Combat Team (HBCT) to improve the durability of M1 Abrams production T-158LL track. A technology transfer agreement (TTA) was implemented with the customer to target improving the durability of T158LL track bushings by 50%.

Comprehensive failure analysis was initiated; track pitches were removed at 250-mile increments over a 3000-mile trial. The primary failure mode for the bushing was rubber fatigue via crack initiation and propagation. This fatigue failure occurs at the unconstrained bushing locations, namely positions 7 & 8 at the center guide followed by positions 1 & 14 at the end connectors (Ref Figure 1A).

Figure 1A: Dissected T-158LL Track Block

Onset of visual cracks in the rubber components (perceived crack initiation) occurs anywhere from ~500-750 miles and propagates; this destroys the load carrying capabilities of the outboard bushings causing the track pins to contact the track block, which leads to failure of the metallic pin.

See Figure 1B for an example of excessive deflection of the track body with respect to the pin.

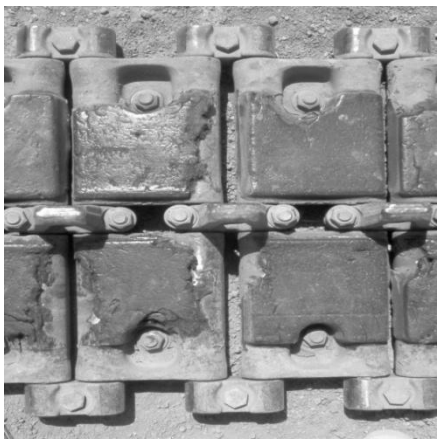

Figure 1B: Bushing failure (excessive gap between track blocks) led to track being "thrown"

Loading Imbalance

These developments led to a systems approach in understanding the factors affecting bushing life,

focusing on backer pad, road wheel, ground pad, and suspension. Early efforts to understand the loading distribution between the backer pad and the road wheel led to the development of the pressure-paper measurement technique.

Environmental and demanding operating conditions contribute to elevating the track pitch temperatures accelerating the degradation of components.

Given that the strength and other key elastomeric properties are diminished at elevated temperatures, it is desirable to minimize the energy generated in the form of heat from the mechanical deflection of the track bushings, ground pads, backer pads and road wheels.

EXPERIMENTAL

Testing Section

Pressure Paper Method Development

Utilizing sensor films and computer analysis allowed for the understanding of load distribution and center of pressure. These results correlated with load cell measurements.

Pressure ranges included:
- Ultra low (28-85 psi)
- Super low (70-350 psi)
- Low (350-1400 psi)

TRADOC Test Protocol

Preferred testing course is Yuma Proving Ground (YPG), Yuma AZ.

- Dynamometer Course:
  - 4 miles per lap
  - Smooth high-strength asphalt
  - 0.8 percent grade
  - 30 ft wide
  - 500 ft radius turnarounds

Operational mode for thermal mapping track components: three complete laps for a total of 12 miles at 45 mph.

Track Switch & Reverse Protocol

Testing protocol from PM Abrams and dictates the T-158LL track is reversed every 500 miles and switched every 1000 miles.

Reversing the track every 500 miles entails disassembling the track on the right and left side of the vehicle, swinging the end of the track until the inboard components replace the position of the original outboard components, then reassembling the track.

Switching the track every 1000 miles entails a reverse procedure in addition to moving the left track to the right side, vice-versa.

Testing Results

An indirect measurement of temperature through Infrared (IR) spectrum radiation corrected with contact thermocouples indicates elevated surface temperature of elastomeric components outboard relative to inboard as shown in Figure 2A.

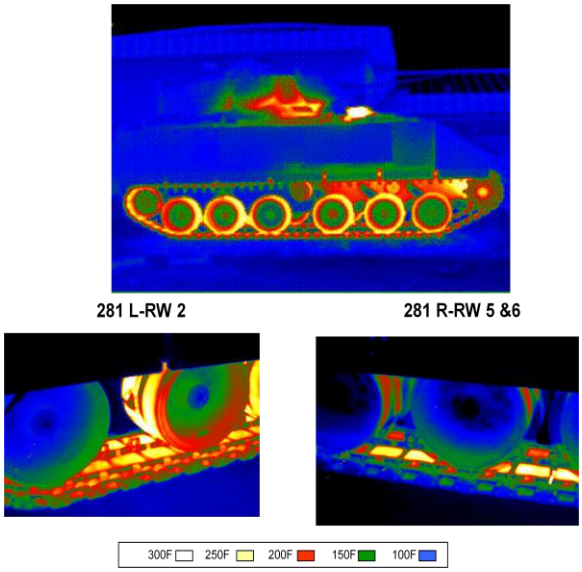

Figure 2A: Example IR measurements, M2 Bradley and M1 Abrams

Reversed Road Arms

Thermal data on the dynamometer course at YPG, three laps at 40mph, revealed a reversal in the outboard/inboard temperature trend (higher inboard temperatures). In addition, pressure paper measurements indicated a reverse trend of higher force on inboard components.

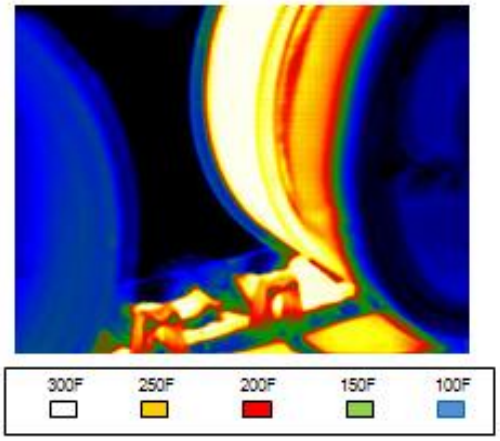

Figure 2B- Thermal Map (Abrams left side - 019)

Investigation into this anomaly revealed the left road arms had been assembled on the right and vice-versa. As a result, instead of the designed one-degree positive camber angle in an unloaded case, the camber angle was negative one-degree camber. This shifted a majority of the vehicle's load to the inboard track and road wheels.

Typical Results

Contact pressure measurements are taken between the road wheel and a steel surface (track off) to maximize test accuracy. Typical results are shown in Figure 3A; intensity of red indicates higher contact pressure.

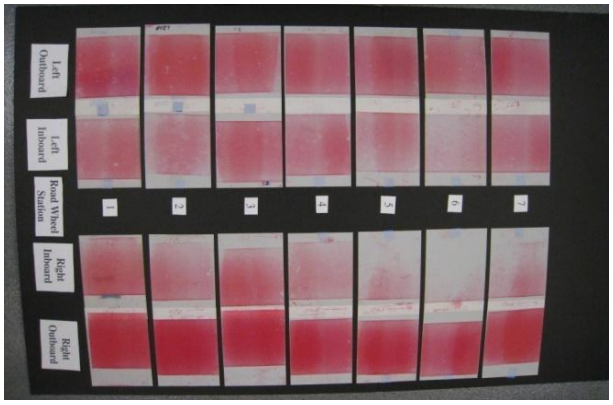

Figure 3A: Contact pressure results M1A1 Abrams

Using pressure paper in Figure 3A, a software product was utilized to convert the red intensity into a pressure profile for the respective road wheel as shown in Figure 3B.

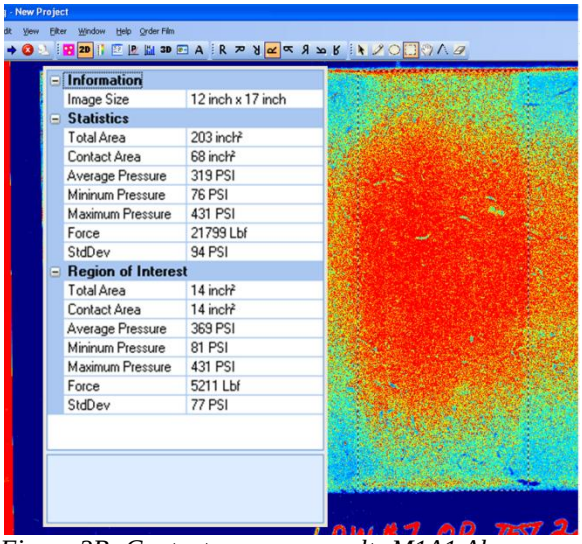

Figure 3B: Contact pressure results M1A1 Abrams

Figure 4 illustrates the correlation between load of the inboard and outboard road wheel stations on the right side of the tank with the corresponding road wheel rubber surface temperatures.

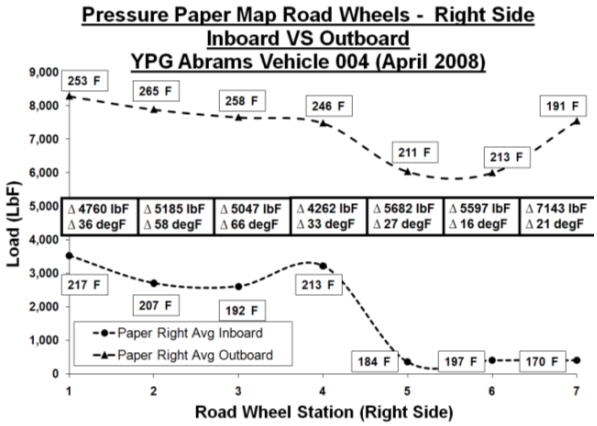

Figure 4: M1 Abrams road wheel loading to temperature correlation following high speed run

The thermal measurements in Figure 4 were immediately recorded after three laps at 40 mph and the higher outboard loads correlate directly with higher surface temperatures. The higher loaded outboard stations experience higher strain, resulting in higher absorbed energy and higher operating temperatures.

Using load cell measurements, a plot of outboard and inboard load versus total load at a given wheel station was created shown in Figure 5.

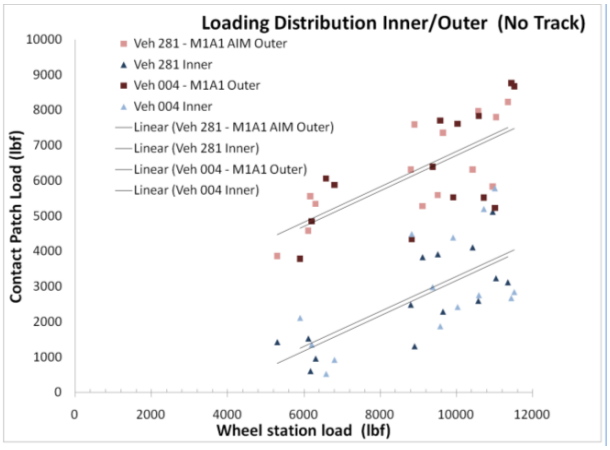

Figure 5: Relationship between total load and inner/outer load balance M1A1

Observed Component Life

Bushing and road wheel backer durability is influenced by the fatigue behavior of the respective rubber components. The fatigue process involves a period of crack nucleation followed by a period, which cracks grow, to a point of failure[6].

Failure depending on the application can be defined as the number of cycles to:

- Cracks of a given size to appear
- Specified stiffness of a specimen
  - increase or decrease
- Rupture of a specimen (hysteresis blowout)
- Loss of material (chunking)

Due to existing test protocol, switching, and reversing the track, Figures 6 & 7 exhibit relatively uniform fatigue for the track components. The test loading profile averages out fatigue inner/outer via the switching and reversing of the track.

The increase in track life has been validated through testing. The practice of switching and reversing the track has been determined to increase track life by approximately 600 miles.

Figure 8 highlights crack initiation in the rubber at bottom and center of the Figure, which leads to bushing failure.

Figure 6: Example embrittlement and cracking of backer pad and bushing assembly M1

Figure 7 shows the progression of embrittlement and loss of material highlighted by white arrows versus component life. Left to right, each sample is at 250 mile increments.

Figure 7: Two examples of the progression of chunking of a backer pad

Figure 8 shows an example of a road wheel near failure.

Figure 8: Example of a nearly failed road wheel; "failure" of a road wheel defined as 50% rubber lost

As discussed above, the life of other track components do not reflect the loading imbalance due to TRADOC test protocol. However, in reviewing road wheel replacement rate from a recent series of tests on four M1A2 Abrams vehicles, road wheel durability confirms this load imbalance between inboard and outboard road wheels. They experience the loading imbalance throughout their life, as they

are not moved from installed position. The data in Figure 9 illustrates the replacement rate of outer road wheels is double the rate of inner.

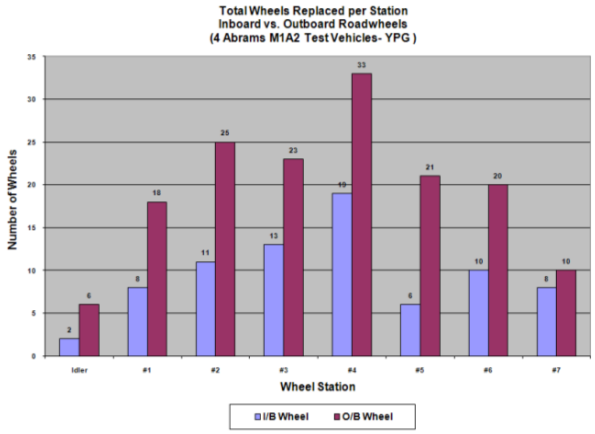

Figure 9: Replacement rate of road wheels at YPG for four M1A2 Abrams vehicles[1]

Fatigue of Natural Rubber (NR)

The analysis of the crack initiation and propagation of elastomers for the prediction of component life (fatigue) is not mature. However, the published research allows for statements regarding the correlation of relationships between factors and life of components.

Example factors of NR component life:

- Temperature
  - Environmental
  - Due to hysteresis
- Loading
  - Strain
    - Max
    - Min
    - Rate
  - Type
    - Complex
    - Shear
    - Tension
    - Compression
- Environment
  - Ozone
  - Oxygen
- Material
  - Strain-crystallizing
  - Stress/Strain relationship

Of the potential factors that are noted, all can change with respect to time as the material undergoes chemical changes. For instance, in a fixed load application, the strain is dependent on the material properties.

Following crack initiation there are three regions of crack propagation in rubber components. The following is paraphrased from "Engineering with Rubber" (Ref 2 and Figure 10).

C is defined as crack length and N is cycle number.

Region 1: Sub-threshold region

- The tearing energy G is less than critical tear energy G_o, the fatigue limit, below this value crack propagation is solely due to ozone.

Region 2: Transition Region

- Crack growth is dependent on both ozone and mechanical factors in an approximately additive and linear fashion.

Region 3: Power Law Regime

- In this region there exists a power law dependency between crack growth rate and G, and has been found for many rubbers and non-rubbery materials.

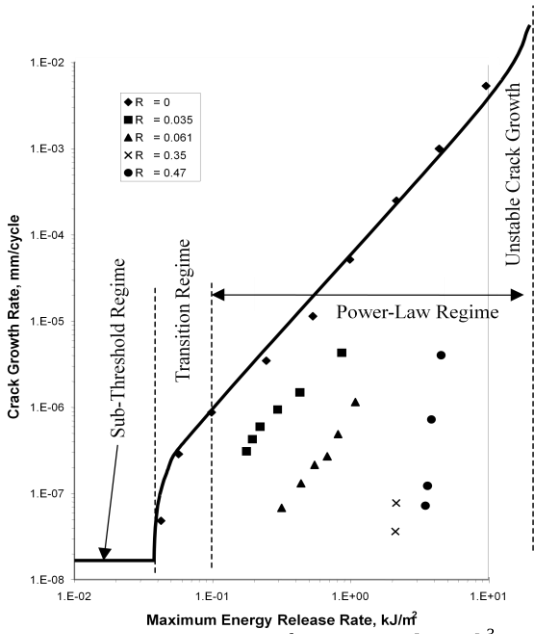

Figure 10: Propagation of an initiated crack[3]

Figures 11 and 12 highlight the dynamic tearing energy and static tearing energy dependence on temperature. These tests are used to understand crack growth rate characteristics and initially have a predefined crack. These relationships can be used to

define the reduction of component life versus temperature.

Figure 11, dynamic case, demonstrates, as temperature is increased, the rate of crack propagation increases.

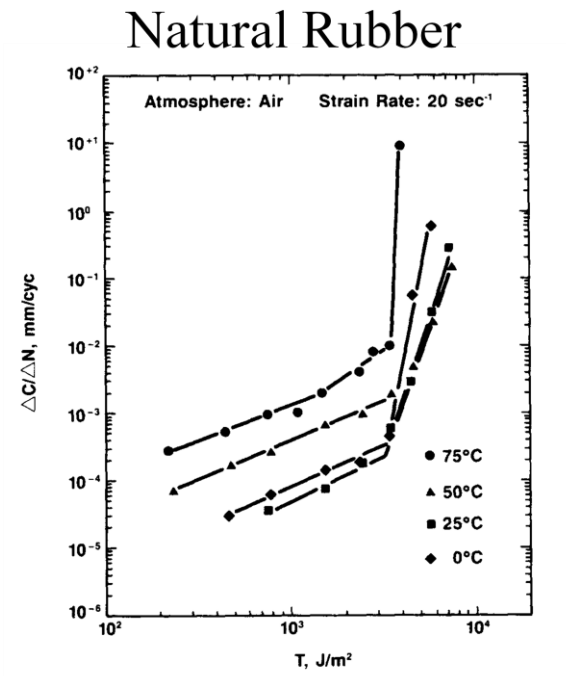

Figure 11: Dependence of crack growth on temperature[4]

Figure 12 shows two material`s tearing strength dependence on temperature. This case was for an initiated crack in planar tension and averaged for three samples.

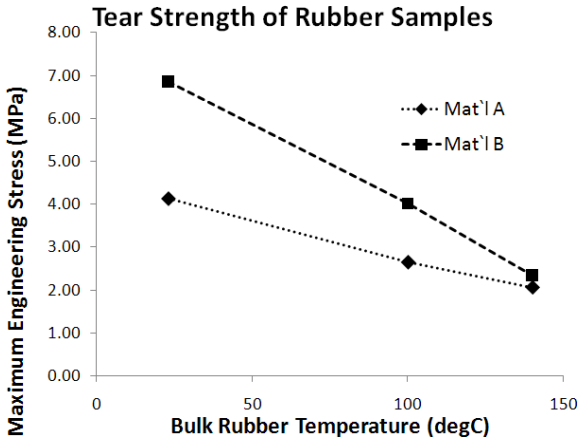

Figure 12: Dependence of static tearing energy on temperature

The relationship of fatigue life to strain field is complicated as shown in Figure 13, however the major components covered in this paper, excluding bushings, cyclically return to zero strain in their application (data points on the vertical axis).

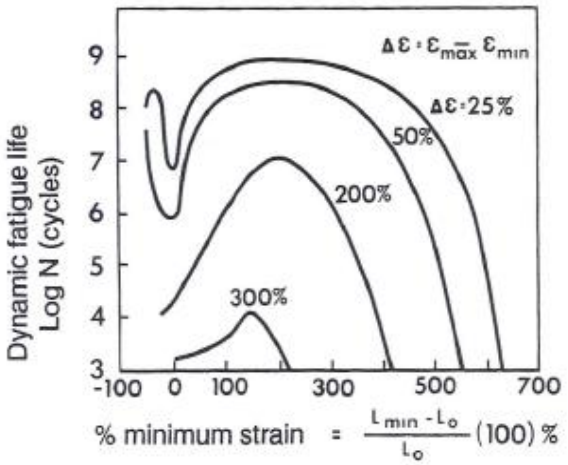

Figure 13: Fatigue life for a NR versus both upper and lower cyclic strain values.[5]

The energy absorption characteristics are defined using the fraction of absorbed strain energy to the elastic strain energy, which is sometimes approximated by taking the tangent of the phase lag between the applied loading displacement/strain and the resulting force/stress.

Currently there is insufficient data collected on the materials used in this system to define the relationship between strain field and temperature above ambient.

MATHEMATICAL MODEL OF SUSPENSION USING FINITE ELEMENT METHOD

Three separate models were developed to understand the suspension assembly and track assembly. Root cause analysis utilized the 3D mock load cell geometry.

3D Suspension Assembly on Mock Load Cells

To speed the solution a 3D model representative of 1/14 of the tank was used to simulate a road wheel station using station`s 3-6 geometry on mock load cells. This was used to calculate the optimum camber angle for inner/outer loading distribution and correlation to available test data.

3D Suspension Assembly Static on Track Assembly

A 3D model of the track assembly was added to verify the loading distribution was minimally affected by the addition of the track and both the total strain energy and the strain energy density fields were approximately uniform inner/outer.

2D Road Wheel Dynamic on Track Assembly

A 2D model was used to estimate the change in component life only due to the change in strain field resulting from the change in loading. The relationship of temperature to strain is not available at this time.

Typical Geometry

Figure 14 shows the 3D geometry of the suspension assembly for the load cell case. A 3D track system was added to this model for the second case, and a 2D planar stress model was created using the geometry and appropriate estimations of section thicknesses.

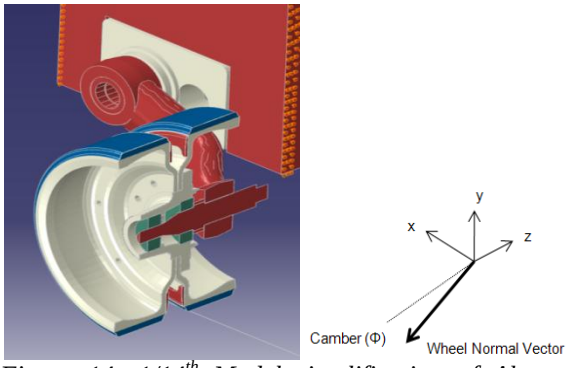

Figure 14: 1/14th Model simplification of Abrams suspension assembly

The camber angle was defined as the angle between the hub normal vector and the x-z plane as show in Figure 14. It was calculated with the equations shown in Figure 15.

$$pta = (a_1, a_2, a_3)$$
$$pta = (b_1, b_2, b_3)$$
$$pta = (c_1, c_2, c_3)$$

$$\overline{ba} = (b_1 - a_1, b_2 - a_2, b_3 - a_3)$$
$$\overline{bc} = (b_1 - c_1, b_2 - c_2, b_3 - c_3)$$

$$\bar{n} = \overline{ba} \times \overline{bc} = (n_1)\hat{i} + (n_2)\hat{j} + (n_3)\hat{k}$$

$$\text{Toe} = \sin^{-1}\left(\bar{n} \cdot \hat{i}\right) = \sin^{-1}\left(\frac{n_1}{|\bar{n}|}\right)$$

$$\text{Camber} = \sin^{-1}\left(\bar{n} \cdot \hat{j}\right) = \sin^{-1}\left(\frac{n_2}{|\bar{n}|}\right)$$

Figure 15: Calculation of camber angle

Material Models

Referencing Figure 14:

- Steel (Red)
  - E= 29,700 ksi
  - ν = .29
- Aluminum (Grey)
  - E=10,000 ksi
  - ν =.33
- Rubbers (Blue)
  - Odgen (N=3) curve fit
  - ν =.5
    - Bushing
    - Backer Pad
    - Road Wheel
    - Ground Pad
- Bearing Material (Green)
  - 1,000 ksi
  - ν =.1

Rubber test data was taken for various compounds used in the track system (historic, current, and future materials (3 samples per material)) and a typical material was selected for each component. The maximum and minimum material models were used for the sensitivity analysis.

Figure 16 shows typical test data that is used to curve fit to mathematical material models.

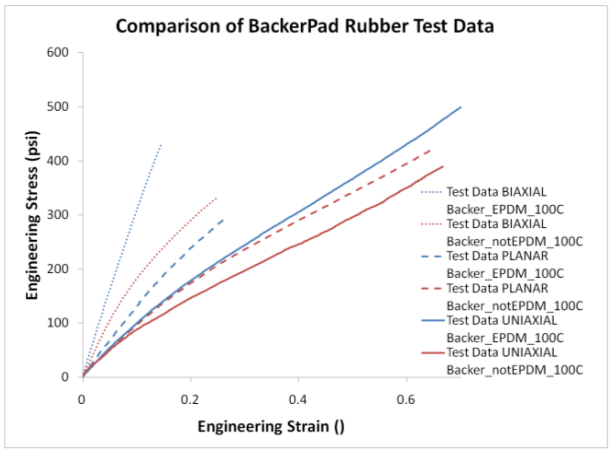

Figure 16: Example Testing Results (three modes of deformation)

The bearing material model used did not affect the resulting load imbalance for the range of reasonable stiffness.

Element Types

- 2nd Order Tet-Modified Formulation
  - Road arm and wear plates
  - Complicated geometry
- 1st order reduced integration points
  - Enhanced Hourglass Control
  - Aluminum road wheel
- 1st order fully integrated brick
  - Rubbers
- 2nd Order Reduced Integration Points
  - All else

Loading Conditions

Suspension Assembly on Mock Load Cells

In order to satisfy the 1/14 chassis simplification: chassis surfaces normal to the x-axis were constrained in the x-direction and the centerline of the chassis was constrained in the z-direction. Mock load cells were given a stiffness of 100,000 lbf/in. A displacement in the y-direction was applied to the centerline of the chassis to achieve the required reaction load at the load cells.

A friction study was completed, there was not an observed relationship between friction levels, and loading distribution, a static coefficient of friction of .4 was chosen.

Suspension Assembly Static on 3D Track Assembly

The boundary conditions for the chassis were the same as the previous case; however, a track system was set under the road wheels to study the effect on loading distribution. The ground pads were bonded to a rigid analytical surface, and a coefficient of static friction of 0.4 was applied between the road wheel and ground pad.

Suspension Assembly Dynamic on 2D Track Assembly

A 2D assembly of only the road wheels and track system for purpose of studying the rolling road wheel across a tensioned track system was created. The boundary conditions were unchanged for friction; however, the loading of the road wheel was load control.

ROOT CAUSE ANALYSIS

Potential factors of loading variance:

- Nominal design (1,0.75,0.5,0.25,0)
  - 1 deg camber (OE Design)
  - 0.3 deg camber (Proposed)
- Measurement error
  - Device
  - Technique
- Geometry variance
  - Avg. not nominal
  - Tolerances (GD&T)
- Materials (esp. elastomers)
- Geometry kinematics
  - Road arm angle
- Environment
  - Vehicle on slope
  - Slope variance

A FEA based sensitivity analysis was used to determine the major factors for loading variance.

Expected maxima and minima of each of the factors above were applied to an average/nominal design and the effect on loading imbalance was noted.

Further analysis is required on “Avg. not nominal” per no manufacturing statistical process control data was available at the time of writing. The assumption that the components utilized are within the design tolerance was assumed.

The major factors regarding loading imbalance were determined to be "Nominal Design" and "Tolerances GD&T." GD&T will be studied to determine cost/benefit relationship of reducing variances due to manufacturing.

RESULTS

Suspension Assembly on Mock Load Cells

Referencing Figure 17, an example simplified geometry; the inner/outer load distribution cannot be uniform at all loads. There is a required moment to bend the road arm to level therefore; initially there will be a higher loading on the outer wheel.

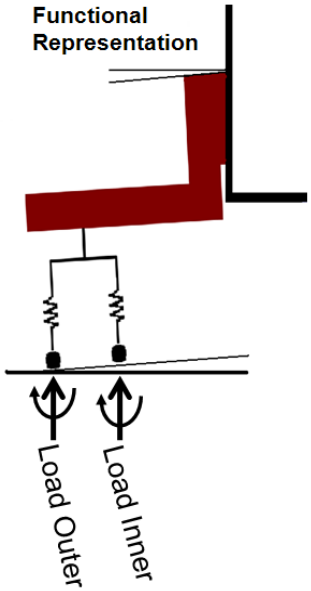

Figure 17: Functional representation of suspension system

As shown in Figure 18, the correlation between the linear curve fits to YPG test data of two different Abrams vehicles to the FEA results of the nominal OE design is strong.

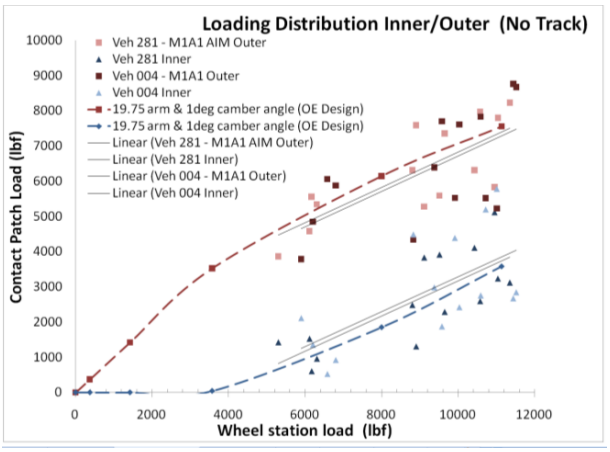

Figure 18: Correlation of YPG test data to FEA

Proposed Solution

As shown in Figure 19, the proposed solution, a reduction of the built in camber angle of the road arm at the road wheel spindle, minimizes the loading imbalance in the loading range of interest (6000lbf – 11000lbf) compared to the OE design.

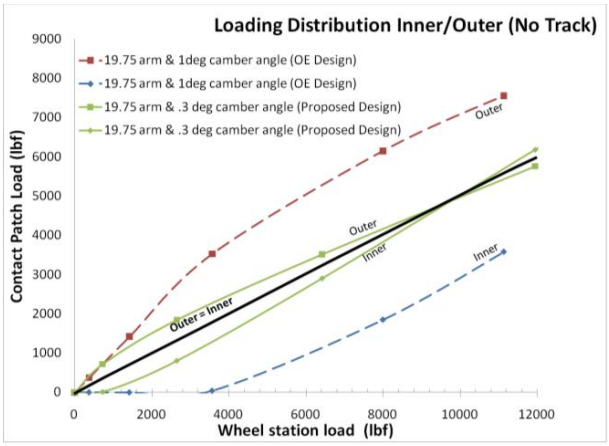

Figure 19: Load distribution OE and proposed

Suspension Assembly Static on 3D Track Assembly

Noting the loading imbalance inner/outer changes due to the applied total loading in the load cell case, a similar result occurs when the track system is used.

Referencing Figure 20, the total strain energy at 9000 lbf was approximately uniform inner/outer as well as the strain energy distribution and loading distribution. The OE design shown in green has a large strain energy imbalance as expected.

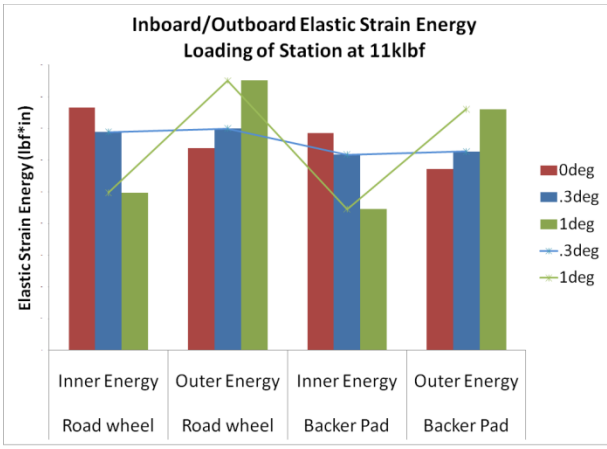

Figure 20: Total strain energy for various camber cases

Suspension Assembly Dynamic on 2D Track Assembly

A 2D analysis was used to understand the relationship between loading and the resulting strain field. The max and min principal strains that each element experiences resulting from 7,500 and 5,500lbf / road wheel load as it traverses across two track blocks is shown in Figure 21. The reduction in load of 50% resulted in a reduction of principal strains of approximately 33%. This was an example of an 11,000-lbf road wheel station, outer road wheel, changing from OE distribution to proposed design distribution.

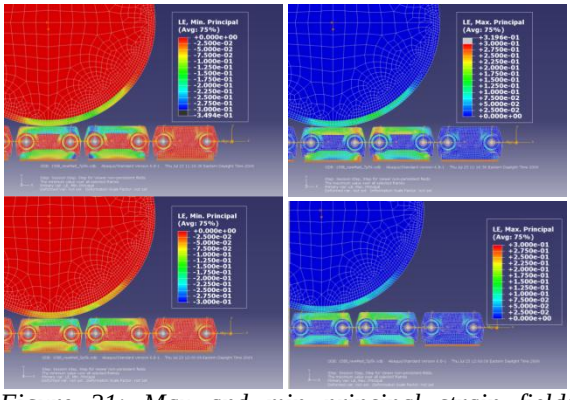

Figure 21: Max and min principal strain fields 7,500lbf and 5,000lbf

DISCUSSION

The strong relationship between camber angle and loading imbalance was evident from testing results and analysis. The testing results` sensitivity to camber angle may be due to the large tolerances on a stack up of many parts.

The nominal design of one deg camber angle inherently loads the outer road wheel greater than the inner road wheel at loads experienced by the wheel stations. Analysis has shown that reducing this angle to .3 degrees reduced the total strain energy, principal strains, strain-energy density, and increases the theoretical life due to the lowering of strain and temperature.

As an example, a M1A1 Abrams loading distribution fraction inner/outer at all road wheel stations at nominal OE design is shown in Figure 22. Using the proposed geometry, the expected loading distribution is shown in Figure 23.

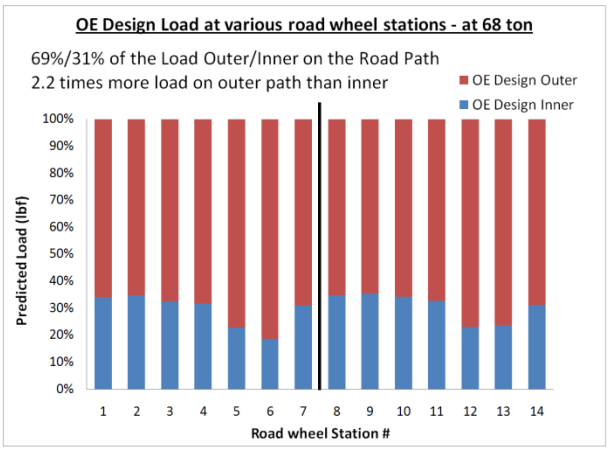

Figure 22: Current nominal loading distribution

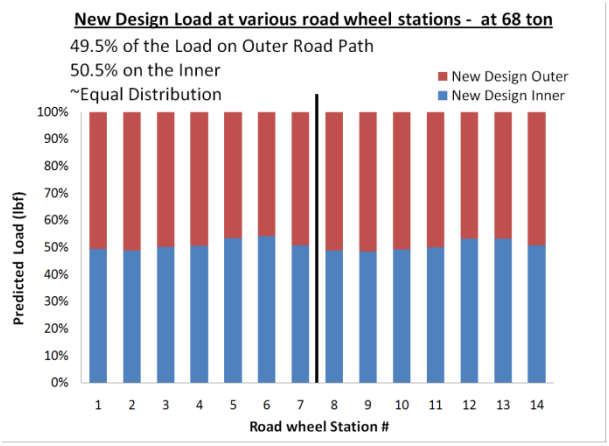

Figure 23: Expected nominal loading distribution

CONCLUSIONS

It was observed through rubber surface temperature, pressure paper, and load cell measurements that the design of the Abrams OE suspension loads the outer track and road wheels greater than the inner.

There is an established relationship between this loading and the heat generation, strain field, and ultimately the replacement rate of the road wheel.

Field data and modeling activities support further investigation is warranted to modify and optimize the road arm camber angle to provide a uniform loading distribution. It is estimated that these improvements will extend the durability of current track components and the life of the track system by lowering both strain and temperature on the outboard components.

ACKNOWLEDGEMENTS

YPG
Alma Arroyo & Jason Green

GDLS
Mark Amato, Ken Nicholson, Joel Litchfield

TARDEC
Special thanks to Bill Dixon, Chuck Coutteau, Bob Smith, & Mike Blain for supporting and assisting our R&D activities.

PM HBCT
Jack Phillips, and Dennis Swears

REFERENCES

- "Road Wheel Durability Summary" Mark Amato 13 July 09 GDLS (2009)
- Gent, A. *Engineering with Rubber* 2nd Ed. HanserGerdner (2001)
- Lindley, *Int. J. Fracture*, 9, 449 (1973)
- Young, *RCT*, 59, 809 (1986)
- Cadwell et al, *Ind. Eng. Chem., Anal. Ed*., 12, 19 (1940)
- W.V. Mars, A. Fatemi; "Fatigue Fracture Engineering Materials Structure," 26, pgs 779-789, 2003.